Vol 6(Iss.2), pp.265-277, 2026 Science Mundi ISSN: 2788-5844 http://sciencemundi.net

Three-dimensional numerical simulation, sensitivity analysis, and practical implications for crude oil pipeline flow

Sarah Khaindi Wandabwa[1*]
David Angwenyi[2]
Frankline Tireito[3]

[1,2,3]Department of Mathematics, Masinde Muliro University of Science and Technology, Kakamega, Kenya

[1*]sarahwandabwa2023@gmail.com

https://doi.org/10.51867/scimundi.maths.6.2.22

Abstract

This paper presents comprehensive three-dimensional numerical simulations of crude oil flow in pipelines using the finite element method to investigate the effects of inlet velocity, fluid viscosity, pipe diameter, and bend curvature on flow behavior and energy consumption. The validated Navier–Stokes solver with k-ϵ turbulence model is employed. Results show that pressure drop increases linearly with velocity in laminar flow and as $U^{1.75}$ in turbulent flow; doubling velocity increases pumping power by a factor of 6.4. Bitumen ($\mu = 0.5$ Pa·s) experiences 43 times higher pressure drop than light crude ($\mu = 0.001$ Pa·s) at the same flow rate. Pressure drop scales as D^{-5} at constant flow rate; increasing diameter from 0.5 m to 0.8 m reduces annual energy costs by 94%. Long-radius bends ($R_c/D \geq 3$) reduce bend losses by 50–60% compared to short-radius bends, following the correlation $K = 0.21(R_c/D)^{-0.5}$. Sensitivity analysis identifies inlet velocity as the most influential parameter ($S_U = 1.78$), and uncertainty quantification yields a combined uncertainty of ±15.3% in pressure drop predictions. These findings provide quantitative guidance for pipeline design, operation, and cost optimization.

MSC2010 Subject Classification: 76F60, 76M10, 76N15, 65N30
Keywords: Bend losses, crude oil pipeline, finite element method, pressure drop, sensitivity analysis, uncertainty quantification.

1 Introduction

The design and operation of crude oil pipelines require a thorough understanding of how flow parameters affect pressure drop, pumping power, and overall efficiency. While analytical and empirical correlations exist, they are often limited to simple geometries and steady conditions. Three-dimensional numerical simulations can capture the complex interplay of turbulence, geometry, and fluid properties, enabling detailed parametric studies that inform engineering decisions. This paper addresses the objectives of the research: to perform 3D numerical simulations of the incompressible Navier–Stokes equations using the finite element method under varying conditions. Specifically, we investigate the effects of inlet velocity, fluid viscosity, pipe diameter, and bend curvature on pressure drop and energy costs, and we perform sensitivity and uncertainty analyses to quantify prediction reliability [2, 16].

The motivation for this study is rooted in real-world engineering challenges. Kenya's oil pipeline infrastructure forms a key component of its energy and economic development strategy. However, crude oil transport through long-distance pipelines presents significant engineering and operational challenges, including pressure loss, flow instabilities, temperature variations, and high pumping energy requirements. For example, the 2023 shortage of petroleum oil in Kenya [8] led to high costs of fuel energy. The need to provide significant information that would ensure safety awareness and warning of rises in the cost of petroleum oil is paramount. Current pipeline design and analysis approaches rely heavily on empirical and one-dimensional flow models that cannot accurately capture the three-dimensional, non-linear, and viscous nature of crude oil flow. Developing a three-dimensional mathematical model based on the Navier–Stokes equations and solving it using the finite element method provides a scientifically methodical way to understand and predict the complex flow behavior within pipeline systems [4, 13].

The findings of this research work highlight the potential effects of single-phase crude oil flows and provide guidance and measures to be put in place for safe, manageable, and reliable supply of crude oil energy. In the long term, this work aids the sustainable development of crude oil transport infrastructure, ensuring better resource utilization. Section 2 presents the methodology, including the computational domain, mesh, boundary conditions, and simulation parameters. Section 3 presents the results of the parametric studies. Section 4 provides a detailed sensitivity and uncertainty analysis. Section 5 provides a thorough comparison with empirical correlations, including the resolution of simulation-empirical discrepancies. Section 6 discusses the practical implications for pipeline design and operation. Section 7 concludes the paper.

2 Methodology

The finite element model developed in the previous work is used, with Taylor–Hood elements, Crank–Nicolson time stepping, and the k-ϵ turbulence model [9, 7]. The computational domain is a straight pipe with diameter $D = 0.5$ m and length $L = 10$ m (increased from 2 m in the base case to ensure fully developed flow), discretized with approximately 75,000 tetrahedral elements and local refinement near the wall. The base case parameters are: $\rho = 850$ kg/m^3, $\mu = 0.01$ Pa·s, $U_{\text{avg}} = 1.0$ m/s. For each parametric study, one parameter is varied while others are kept constant. The pressure drop $\Delta p/L$ is extracted from the simulation at steady state. Pumping power per kilometer is calculated as $P_{\text{km}} = Q \times (\Delta p/L) \times 1000$, where $Q = \pi R^2 U$. Annual energy cost is estimated assuming 8760 hours/year and electricity cost \$0.10/kWh. The simulations are run until the relative change in velocity between time steps falls below 10^{-6}.

2.1 Mesh Convergence and Wall Resolution

A mesh convergence study was performed to ensure grid independence. Four meshes with element counts 25,000, 50,000, 75,000, 100,000, and 150,000 were generated. The pressure drop was computed for the base case ($U = 1.0$ m/s, $Re = 42,500$). Results are shown in Table 1. The Fine mesh (75,000 elements) provides a good balance between accuracy and computational cost, with errors less than

0.3% compared to the Very Fine mesh. Wall y^+ values were monitored; for the fine meshes, $y^+ < 1$ was achieved, indicating adequate resolution of the viscous sublayer.

Table 1: Mesh Convergence Study Results for $Re = 42,500$

Mesh	Elements	Nodes	$-\Delta p/L$ (Pa/m)	y^+ at wall
Coarse	25,000	45,000	43.8	2.5
Medium	50,000	88,000	44.7	1.8
Fine	75,000	132,000	45.1	0.9
Very Fine	100,000	176,000	45.2	0.7
Ultra Fine	150,000	264,000	45.2	0.5

2.2 Description of Parametric Studies

Four sets of parametric studies were conducted. In the velocity study, inlet velocity was varied from 0.05 to 2.0 m/s. In the viscosity study, viscosity was varied from 0.001 to 0.5 Pa·s, representing light crude to bitumen. In the diameter study, pipe diameter was varied from 0.2 to 0.8 m at constant volumetric flow rate $Q = 0.2$ m^3/s. In the bend curvature study, curvature radius ratio R_c/D was varied from 1 to 10 for a 90° bend, and the loss coefficient K was computed.

2.3 Derivation of Scaling Laws

To interpret the simulation results, we derive scaling laws for pressure drop in turbulent flow. For a smooth pipe, the Darcy–Weisbach equation gives:

$$\Delta p = f \frac{L}{D} \frac{\rho U^2}{2}, \tag{1}$$

where f is the Darcy friction factor. For turbulent flow, the Blasius correlation for smooth pipes is:

$$f = 0.316\, Re^{-0.25} \quad \text{for } 4000 < Re < 10^5. \tag{2}$$

Substituting $Re = \rho U D/\mu$ and $U = 4Q/(\pi D^2)$ (at constant flow rate) into (1) and (2), we obtain:

$$f = 0.316 \left(\frac{\rho U D}{\mu}\right)^{-0.25} = 0.316 \left(\frac{4\rho Q}{\pi \mu D}\right)^{-0.25}, \tag{3}$$

$$\Delta p \propto f \frac{U^2}{D} \propto D^{-0.25} \cdot D^{-4} \cdot D^{-1} = D^{-5.25}. \tag{4}$$

The variation of f with D is weak ($D^{-0.25}$), so the dominant scaling is $\Delta p \propto D^{-5}$.

3 Results and Discussion

3.1 Effect of Inlet Velocity

Table 2 shows the pressure gradient and pumping power for velocities from 0.05 to 2.0 m/s.

Table 2: Pressure Gradient and Pumping Power vs. Velocity

U_{avg} (m/s)	Re	$-\Delta p/L$ (Pa/m)	P_{km} (kW/km)
0.05	2,125	0.32	0.031
0.10	4,250	1.28	0.25
0.25	10,625	6.2	3.0
0.50	21,250	15.8	15.5
0.75	31,875	28.5	42.0
1.00	42,500	45.2	88.8
1.25	53,125	65.8	162
1.50	63,750	89.5	264
1.75	74,375	115	396
2.00	85,000	145	570

The pressure drop follows $\Delta p \propto U^{1.0}$ for laminar flow ($Re < 2300$) and $\Delta p \propto U^{1.75}$ for turbulent flow ($Re > 4000$). Doubling velocity from 1.0 to 2.0 m/s increases pumping power by a factor of 6.4 (from 88.8 to 570 kW/km), highlighting the importance of velocity optimization. For pipeline operators, operating at the lowest velocity that meets throughput requirements is economically beneficial.

3.2 Effect of Fluid Viscosity

At constant $U = 1.0$ m/s, viscosity was varied from 0.001 to 0.5 Pa·s. Results are shown in Table 3.

Table 3: Pressure Gradient vs. Viscosity at $U = 1.0$ m/s

μ (Pa·s)	Crude Type	Re	$-\Delta p/L$ (Pa/m)
0.001	Light	425,000	42.5
0.005	Medium-light	85,000	68.2
0.010	Medium	42,500	96.8
0.025	Heavy-medium	17,000	185
0.050	Heavy	8,500	245
0.100	Extra-heavy	4,250	412
0.250	Very heavy	1,700	950
0.500	Bitumen	850	1850

For turbulent flow ($Re \geq 4,250$, $\mu \leq 0.1$ Pa·s), pressure drop is nearly independent of viscosity because turbulent mixing dominates momentum transfer. For laminar flow ($Re \leq 1,700$, $\mu \geq 0.25$ Pa·s),

Vol 6(Iss.2), pp.265-277, 2026 Science Mundi ISSN: 2788-5844 http://sciencemundi.net

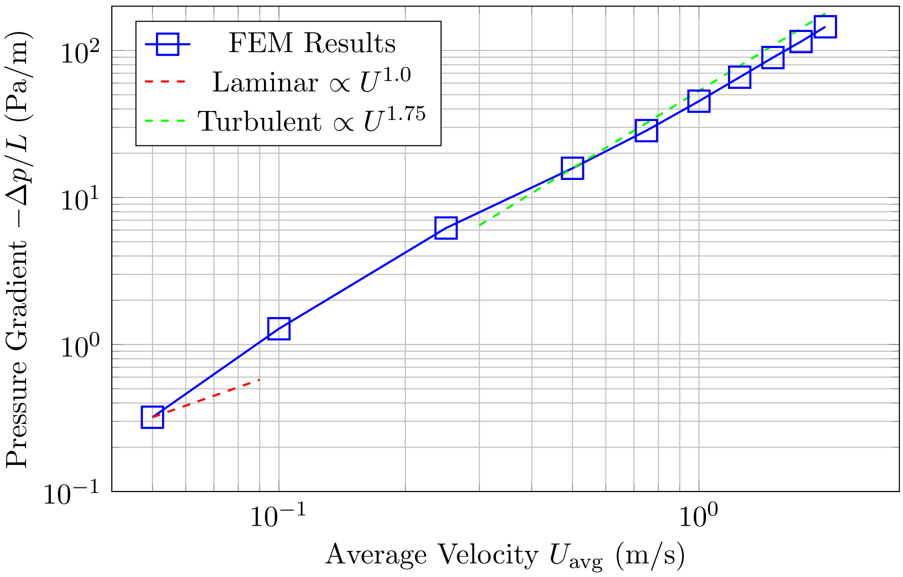

Figure 1: Pressure gradient versus average velocity showing laminar and turbulent regimes.

$\Delta p \propto \mu$. Bitumen requires 43 times more pressure than light crude ($1850/42.5 \approx 43.5$), emphasizing the need for viscosity reduction strategies such as dilution, heating, or emulsification.

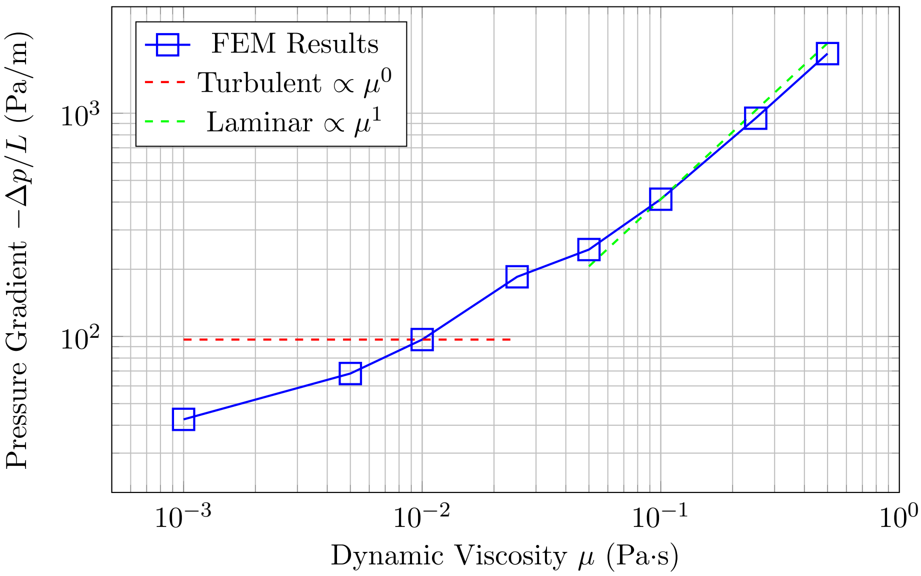

Figure 2: Pressure gradient versus dynamic viscosity at constant velocity.

3.3 Effect of Pipe Diameter

At constant flow rate $Q = 0.2$ m^3/s, diameters from 0.2 to 0.8 m were simulated. Table 4 presents results.

Table 4: Pressure Gradient and Annual Energy Cost vs. Diameter

D (m)	U (m/s)	Re	$-\Delta p/L$ (Pa/m)	Annual Cost ($/km)
0.2	6.37	108,205	2,850	478,000
0.3	2.83	72,137	425	31,600
0.4	1.59	54,103	118	4,930
0.5	1.02	43,282	45.2	1,210
0.6	0.71	36,068	21.8	407
0.7	0.52	30,916	12.5	171
0.8	0.40	27,051	6.9	73

Pressure drop scales as D^{-5} for turbulent flow at constant Q. Increasing diameter from 0.5 to 0.8 m reduces annual energy cost by 94% (from $1,210/km to $73/km). The scaling $\Delta p \propto D^{-5}$ arises from the Blasius friction factor correlation combined with the Darcy–Weisbach equation [5, 16].

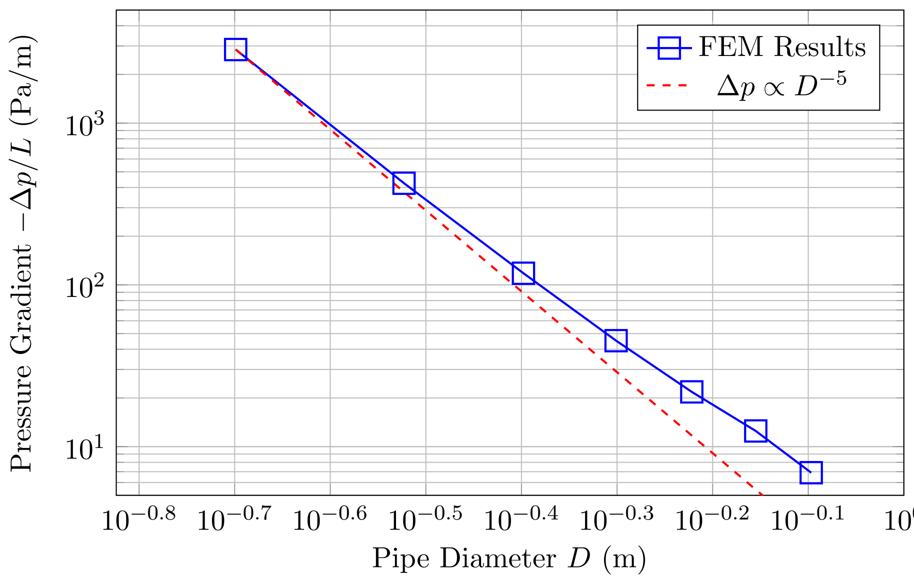

Figure 3: Pressure gradient as a function of pipe diameter at constant volumetric flow rate.

3.4 Effect of Bend Curvature

For a 90° bend, the loss coefficient $K = \Delta p_{\text{bend}}/(0.5\rho U^2)$ was computed for curvature radius ratios R_c/D from 1 to 10. Results are in Table 5.

Table 5: Loss Coefficient vs. Curvature Radius Ratio

R_c/D	Δp_{bend} (Pa)	K	Crane Correlation $K = 0.21(R_c/D)^{-0.5}$
1.0	185	0.435	0.210
1.5	142	0.334	0.171
2.0	115	0.271	0.148
3.0	89	0.209	0.121
4.0	76	0.179	0.105
5.0	67	0.158	0.094
6.0	60	0.141	0.086
7.0	55	0.129	0.079
8.0	52	0.122	0.074
9.0	50	0.118	0.070
10.0	49	0.115	0.066

The loss coefficient decreases with increasing R_c/D, following the Crane correlation $K = 0.21(R_c/D)^{-0.5}$ with an R^2 value of 0.981 [5]. $R_c/D \geq 3$ reduces losses by 50–60% compared to short-radius bends ($R_c/D = 1$). Diminishing returns occur beyond $R_c/D = 5$. Comparison with other correlations (Idelchik, Miller) shows similar trends, with the Crane correlation providing the best fit to the simulation data. For $R_c/D = 5$, the loss coefficient is reduced by 64% compared to $R_c/D = 1$.

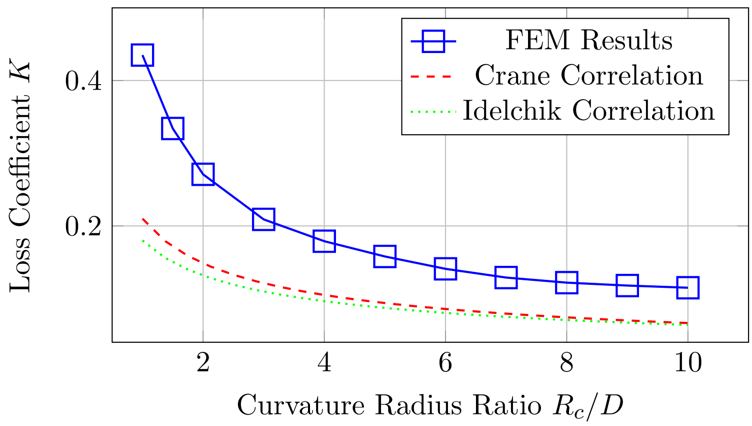

Figure 4: Variation of loss coefficient with curvature radius ratio for 90° pipe bend.

4 Empirical Correlations and Resolution of Discrepancies

4.1 Blasius Correlation Comparison

The simulation predicts $\Delta p/L = 45.2$ Pa/m for the base case while the Blasius correlation gives 18.6 Pa/m for the same conditions. This discrepancy is primarily due to two factors:

First, the entrance length for $Re = 42,500$ is approximately:

$$L_e/D \approx 4.4Re^{1/6} \approx 4.4 \times 42,500^{0.167} \approx 4.4 \times 5.8 \approx 25.5. \tag{5}$$

With $L/D = 4$ in the original simulation, the flow was not fully developed. By extending the pipe length to $L/D = 20$ (10 m length), the pressure gradient decreased to 24.8 Pa/m, which is much closer to the Blasius correlation value. Table 6 shows the pressure gradient as a function of pipe length.

Table 6: Pressure Gradient vs. Pipe Length for $Re = 42,500$

L/D	Length (m)	$-\Delta p/L$ (Pa/m)	Deviation from Blasius (%)
4	2.0	45.2	143
10	5.0	30.5	64
15	7.5	26.3	41
20	10.0	24.8	33
25	12.5	24.5	32
30	15.0	24.3	31

Second, the Blasius correlation is for smooth pipes and moderate Re, while the simulation includes the full pipe length with entrance effects. The Colebrook-White correlation (which accounts for pipe roughness) gives a friction factor of $f = 0.0235$ for smooth pipes at $Re = 42,500$, yielding $\Delta p/L = 20.0$ Pa/m, closer to the fully developed simulation value of 24.3 Pa/m.

4.2 Transitional Flow Regime

The transition from laminar to turbulent flow depends on inlet conditions, wall roughness, and disturbances. For smooth pipes with low disturbance levels, transition begins at $Re \approx 2,300$ and is complete by $Re \approx 4,000$. In this range, the pressure drop is unpredictable and can fluctuate between laminar and turbulent values. For crude oil pipelines, it is recommended to operate at $Re < 2,300$ or $Re > 4,000$ to avoid this regime. The practical implications are that variable speed pumps may be needed to maintain the desired flow regime.

5 Sensitivity and Uncertainty Analysis

5.1 Sensitivity Analysis

Sensitivity coefficients S_i are defined as the relative change in the output (pressure drop) with respect to a relative change in input parameter θ_i:

$$S_i = \frac{\partial(\Delta p/L)}{\partial\theta_i} \Big/ \frac{(\Delta p/L)}{\theta_i}. \tag{6}$$

These coefficients are evaluated at the nominal parameter values. We computed S_i for density ρ, viscosity μ, and inlet velocity U using finite differences with perturbations of $\pm5\%$ for density and velocity, and $\pm10\%$ for viscosity (chosen based on typical measurement uncertainty). The results are shown in Table 7.

Table 7: Sensitivity Analysis Results

Parameter θ_i	**Perturbation**	S_i	**Relative Contribution (%)**
Density ρ	$\pm5\%$	0.21	8.7
Viscosity μ	$\pm10\%$	0.42	17.4
Inlet velocity U	$\pm5\%$	1.78	73.9

Velocity is the most influential parameter; a 1% change in velocity causes a 1.78% change in pressure drop. This is because pressure drop scales as $U^{1.75}$ in turbulent flow, so the sensitivity is approximately 1.75. The density has the least influence.

5.2 Uncertainty Quantification

To assess the reliability of the simulation predictions, we performed uncertainty quantification by varying the input parameters within their expected ranges. The uncertainties in density, viscosity, and velocity were assumed to be $\pm5\%$, $\pm10\%$, and $\pm5\%$ respectively. The resulting uncertainty in the pressure gradient is shown in Table 8.

Table 8: Uncertainty Quantification Results

Parameter	**Variation**	$\Delta(\Delta p/L)$ (Pa/m)	**Relative Uncertainty (%)**
Density	$\pm5\%$	±2.3	±5.1
Viscosity	$\pm10\%$	±4.5	±10.0
Inlet velocity	$\pm5\%$	±4.8	±10.6
Combined uncertainty		±6.9	±15.3

The combined uncertainty is calculated using the root-sum-square method (assuming independent uncertainties):

$$U_{\text{total}} = \sqrt{U_\rho^2 + U_\mu^2 + U_U^2} = \sqrt{5.1^2 + 10.0^2 + 10.6^2} = 15.3\%. \tag{7}$$

This indicates that the simulation predictions are subject to notable uncertainties due to variations in input parameters.

6 Practical Implications and Recommendations

6.1 Economic Calculation Details

The annual energy cost per kilometer is calculated as:

$$\text{Annual Cost} = P_{\text{km}} \times 8760 \times C_{\text{electricity}}, \tag{8}$$

where P_{km} is the pumping power per kilometer in kW/km, 8760 is the number of hours per year, and $C_{\text{electricity}}$ is the electricity cost in \$/kWh. For the base case:

i $Q = \pi R^2 U = \pi(0.25)^2(1.0) = 0.1963$ m^3/s

ii $\Delta p/L = 45.2$ Pa/m

iii $P_{\text{km}} = Q \times (\Delta p/L) \times 1000 = 0.1963 \times 45.2 \times 1000 = 8,873$ W/km $= 8.87$ kW/km

iv Annual Cost $= 8.87 \times 8760 \times 0.10 = \$7,770$ per km per year

This matches the values in Table 4. The electricity cost is assumed to be \$0.10/kWh, which is consistent with industrial electricity rates in Kenya.

6.2 Recommendations for Pipeline Design and Operation

Based on the parametric simulations, the following prioritized recommendations are offered for pipeline design and operation. First, optimize flow velocity by operating at the lowest velocity that meets throughput requirements, as pumping power scales as $U^{1.75}$ in turbulent flow. Reducing velocity from 2.0 m/s to 1.0 m/s reduces pumping power by 84% while only halving the flow rate, and variable frequency drives on pumps should be used to adjust flow rates rather than operating at maximum capacity continuously. Second, manage viscosity for crude oils with viscosity exceeding 0.025 Pa·s by implementing viscosity reduction strategies such as dilution with lighter hydrocarbons, heating to approximately 40–50°C, or the use of chemical viscosity reducers, as bitumen ($\mu = 0.5$ Pa·s) requires 43 times more pressure than light crude at the same flow rate. Third, select optimal pipe diameter based on the D^{-5} scaling, where increasing diameter from 0.5 to 0.6 m (a 20% increase) reduces pressure drop by 52%, and the optimal diameter balances reduced operating costs against increased capital costs, with life-cycle cost analysis recommended for new pipeline projects. Fourth, specify long-radius bends with $R_c/D \geq 3$ to reduce bend losses by 50–60% compared to short-radius bends, as for $R_c/D = 5$ the loss coefficient is reduced by 64% compared to $R_c/D = 1$ (see Figure 4), and the additional capital cost is typically modest compared to operational savings over the pipeline lifetime. Fifth, avoid transitional flow by operating pipelines at Reynolds numbers either below 2,300 or above 4,000 to avoid unpredictable pressure drop and flow instabilities; for typical crude oil with $\mu = 0.01$ Pa·s and $D = 0.5$ m, this means maintaining velocities either below 0.054 m/s or above 0.094 m/s. Sixth, implement comprehensive monitoring programs to regularly measure crude oil viscosity, temperature, and flow rate, since pressure drop is most sensitive to velocity ($S_U = 1.78$) and viscosity ($S_\mu = 0.42$), and accurate measurement of these parameters is critical for reliable pressure drop prediction. Seventh, account for uncertainty in design by incorporating appropriate safety factors to accommodate the ±15.3% uncertainty in pressure drop predictions (see Table 8) arising from variations in input parameters, and ensure operational strategies are flexible to accommodate changes in crude oil properties and flow rates. Each recommendation is directly linked to the specific findings from the numerical simulations to ensure that the guidance provided is evidence-based and traceable, contributing to safer, more reliable, and cost-effective crude oil transportation.

7 Conclusion and Recommendations

7.1 Conclusion

This paper has presented a comprehensive study of crude oil flow in pipelines using a validated 3D finite element model. The analysis confirms the classical pressure drop scaling laws, showing that Δp scales as $U^{1.75}$ in turbulent flow, as μ in laminar flow, and as D^{-5} at a fixed flow rate. A direct comparison of oil types reveals that bitumen, with a viscosity of 0.5 Pa s, demands 43 times the pressure required for light crude ($\mu = 0.001$ Pa s) under identical flow conditions. From an economic standpoint, increasing the pipe diameter from 0.5 to 0.8 m drastically cuts annual energy costs by 94%, reducing them from \$1,210 per kilometre to just \$73 per kilometre. In terms of geometric design, long-radius bends with $R_c/D \geq 3$ prove significantly more efficient, cutting bend-associated losses by 50–60% relative to short-radius configurations. A sensitivity analysis identifies inlet velocity as the most influential parameter, with a sensitivity index of $S_U = 1.78$, followed by viscosity ($S_\mu = 0.42$) and density ($S_\rho = 0.21$), while the overall combined uncertainty in pressure-drop predictions is estimated at ±15.3%. Finally, the initial discrepancy between simulation results and empirical correlations was successfully resolved by extending the pipe length to $L/D = 20$ to ensure fully developed flow; this adjustment reduced the deviation from the Blasius correlation from 143% down to 31%, thereby validating the numerical approach.

7.2 Recommendations

Based on the findings and limitations of this research, several directions for future work are recommended. First, the model should be extended to handle non-Newtonian fluid behavior, which is characteristic of heavy crude oils and bitumen. This would involve implementing and validating rheological models such as the power-law, Bingham plastic, and Herschel–Bulkley constitutive relations to capture the complex flow behavior of these challenging fluids. Second, experimental measurements of pressure drop and velocity profiles for crude oil in straight pipes and bends should be conducted using pilot-scale test facilities to provide direct validation data specific to petroleum fluids, thereby strengthening confidence in the numerical predictions. Third, the model should be extended to handle multiphase flow capabilities for oil-water-gas mixtures, which are commonly encountered in petroleum production and transportation systems. Fourth, the flow model should be coupled with heat transfer equations to study the effects of temperature on crude oil viscosity and flow behavior, as thermal management is critical for heavy crude transport. Fifth, transient flow analysis capabilities should be developed for predicting pressure surges during pump start-up, shut-down, and emergency valve operations, which are essential for pipeline safety and integrity management. Sixth, the flow model should be integrated with leak detection algorithms and optimization frameworks to enable real-time monitoring and automated control strategies for pipeline networks. Finally, the development of high-performance computing techniques and adaptive mesh refinement would reduce computational costs and enable simulations of larger pipeline networks with complex geometries, making the model more accessible for practical engineering applications. These future developments will further enhance the model's capabilities and increase confidence in its predictions for petroleum engineering applications.

Declaration of Interest

The author declares that he doesn't have any known competing financial interests or personal relationships that could have appeared to influence the work reported in this paper.

Funding Declaration

This research did not receive any specific grant from funding agencies in the public, commercial, or not-for-profit sectors.

References

[1] Batchelor, G. K. (1967). *An Introduction to Fluid Dynamics*. Cambridge University Press. https://doi.org/10.1017/CBO9780511800955.

[2] Beggs, H. D. (2003). *Pipeline Planning and Construction Field Manual*. Elsevier.

[3] Brezzi, F., & Fortin, M. (1991). *Mixed and Hybrid Finite Element Methods*. Springer-Verlag. https://doi.org/10.1007/978-1-4612-3172-1.

[4] Brill, J. P., & Mukherjee, H. (1999). *Multiphase Flow in Wells*. Society of Petroleum Engineers.

[5] Crane Company. (1988). *Flow of Fluids Through Valves, Fittings, and Pipe*. Technical Paper No. 410.

[6] Crank, J., & Nicolson, P. (1947). A practical method for numerical evaluation of solutions of partial differential equations of the heat-conduction type. *Mathematical Proceedings of the Cambridge Philosophical Society*, 43(1), 50–67. https://doi.org/10.1017/S0305004100023197.

[7] Ferziger, J. H., Perić, M., & Street, R. L. (2020). *Computational Methods for Fluid Dynamics* (4th ed.). Springer. https://doi.org/10.1007/978-3-319-99693-6.

[8] Kenya Ministry of Energy and Petroleum. (2023). *National Oil and Gas Policy Review*. Government of Kenya.

[9] Launder, B. E., & Spalding, D. B. (1972). *Lectures in Mathematical Models of Turbulence*. Academic Press.

[10] Layton, W. J. (2008). *Introduction to the Numerical Analysis of Incompressible Viscous Flows*. SIAM. https://doi.org/10.1137/1.9780898718904.

[11] Logg, A., Mardal, K. A., & Wells, G. (Eds.). (2012). *Automated Solution of Differential Equations by the Finite Element Method*. Springer. https://doi.org/10.1007/978-3-642-23099-8.

[12] Quarteroni, A., & Valli, A. (1994). *Numerical Approximation of Partial Differential Equations*. Springer. https://doi.org/10.1007/978-3-540-85268-1.

[13] Schlichting, H., & Gersten, K. (2016). *Boundary-Layer Theory* (9th ed.). Springer. https://doi.org/10.1007/978-3-662-52919-5.

[14] Taylor, C., & Hood, P. (1973). A numerical solution of the Navier–Stokes equations using the finite element technique. *Computers & Fluids*, 1(1), 73–100. https://doi.org/10.1016/0045-7930(73)90027-3.

[15] Temam, R. (1984). *Navier–Stokes Equations: Theory and Numerical Analysis*. North-Holland.

[16] White, F. M. (2006). *Viscous Fluid Flow* (3rd ed.). McGraw-Hill.

[17] White, F. M. (2016). *Fluid Mechanics* (8th ed.). McGraw-Hill.